




One-way deep indoor positioning system for conventional GNSS receiver using paired transmitters

Minhuck Park¹  | Jin-Hee Han² | O-Jong Kim³  | Jungbeom Kim³  | Changdon Kee¹

¹ Department of Aerospace Engineering and the Institute of Advanced Machines and Design, Seoul National University, Seoul, Republic of Korea

² Danam Systems Inc., Anyang, Republic of Korea

³ System LSI Business, Samsung Electronics, Hwaseong, Republic of Korea

Correspondence

Changdon Kee, Department of Aerospace Engineering and the Institute of Advanced Machines and Design, Seoul National University, Seoul, Republic of Korea.
Email: kee@snu.ac.kr

Funding information

Ministry of Science and ICT, Republic of Korea, Grant/Award Number: 2020M3C1C1A01086407

Abstract

Generally, GNSS-based indoor navigation systems use repeaters or pseudolites. However, these methods are vulnerable to multipath errors and require additional information, including the repeater or pseudolite position. In this study, we propose a novel one-way indoor positioning system using GNSS signal transmitters. Our system uses paired transmitters, each of which broadcasts the same set of satellite signals. The autocorrelation functions of the combined signals are analyzed as the overlap of each individual autocorrelation function. The estimated position can be determined along the track between the transmitters. The multipath error is absorbed by the clock bias and does not cause position bias error. Furthermore, the proposed system can be applied in current commercial GNSS receivers directly. A theoretical analysis of the pseudorange, user position, multipath error, and signal power is included and supported by simulation results. A field test was conducted to confirm the feasibility of the proposed system.

KEYWORDS

indoor navigation, transmitter, auto-correlation function

1 | INTRODUCTION

As the necessity of indoor positioning has emerged, various positioning methods have been proposed, such as wireless local area network-based or WIFI-based (Landa et al., 2019; Mazuelas et al., 2009; Syed & Arslan, 2011), ultra-wideband-based (Kok et al., 2015; Pagès & Vilà-Valls, 2019; Yan et al., 2013), radio-frequency identification-based (Saab & Nakad, 2011; Tang & Kim, 2010), Bluetooth-based (Ai et al., 2019), and long-term evolution-based (Abdallah et al., 2019; Shin et al., 2019) algorithms. Each of these algorithms has pros and cons (Mautz, 2012), and a suitable method may vary depending on the indoor environment and the user. Various indoor positioning algorithms exist because the Global Navigation Satellite System (GNSS), a

powerful positioning method outdoors, cannot be easily used indoors.

To deploy GNSS signals indoors, various studies have been conducted. When a signal transmitted by a specific satellite is received indoors, the signal strength decreases as it passes through a window, and signal distortion, such as reflection, diffraction, and scattering, occurs. To address these problems, the assisted-Global Positioning System (GPS) method has been introduced, and increasing integration time for weak signal tracking and massive parallel methods for reducing calculation time have been proposed in receiver algorithms (Lachapelle, 2004; Zhang et al., 2010). However, these methods cannot be employed in a deep indoor environment where no actual satellite signal is received.

To exploit GNSS signals in such deep indoor environments, a pseudolite-based or repeater-based indoor positioning method has been introduced. The pseudolite generates a pseudorandom noise (PRN) code that is similar to an authentic GNSS signal; hence, the user can receive the satellite signals. The user can calculate the navigation solution in the same way as GNSS. However, because the user receives signals from a pseudolite installed at several points, the multipath error is large, and near-far problems arise from a large signal strength difference for each pseudolite, depending on the user position. To address these problems, multipath reduction studies using a carrier phase measurement – which is more robust to multipath than a pseudorange – as well as a pulsing technique for alleviating the near-far problem, have been conducted (Kee et al., 2003). In addition, single station-based indoor positioning system studies using multiple antenna arrangements have been carried out to solve the integer ambiguity easily (Kim & Kee, 2019; Kim et al., 2019). To calculate the position, however, the user needs to know the pseudolite position. Furthermore, to avoid the duplication of the actual PRN code, the receiver should be altered to the tracking mode, or a new PRN code should be assigned. Therefore, an additional navigation filter is necessary, which implies that the customary GNSS receiver cannot be applied directly.

In repeater-based indoor positioning systems, research has been conducted to avoid signal overlapping between repeaters or to distinguish repeaters. Ozsoy et al. (2013) proposed a method for avoiding signal overlapping by broadcasting different satellite signals for each repeater using a directional GPS antenna and low noise amplifiers. In their study, the user position can be determined by removing the distance between repeaters and satellites exploiting the known repeater position from the received pseudoranges. A method for distinguishing repeaters is to use the switching of four repeaters connected to one external antenna (Jee et al., 2004, 2005). In these studies, the pseudorange difference between repeaters is calculated by the phase offset generated during the switching process. To solve the discontinuity problem of measurements, which is a disadvantage of the above studies, a method of separating the repeater signal by delaying the signal by more than one chip has been proposed (Im et al., 2006). To increase position accuracy, Jardak and Samama (2009) demonstrated that it is possible to reduce receiver noise by applying an open code loop. In addition, research has been conducted to distinguish repeaters by controlling the signal delay using the cable length (Vervisch-Picois & Samama, 2009). Li (2019) proposed a method for distinguishing repeaters without sequential switching and without adjusting the cable length by broadcasting signals from four independently installed repeaters. In repeater-based indoor posi-

tioning, the user needs to know prior information, such as the repeater position or the signal delay between repeaters. Similar to pseudolite-based indoor positioning, an additional navigation filter is required, and it is also vulnerable to multipath errors.

In this study, we propose a new indoor positioning system based on two transmitters similar to a repeater. The transmitter is a device that broadcasts simulated signals that would be received at the location of the transmitter itself based on ephemeris and timing information received through a data network or nearby GNSS receiver with a pulse-per-second (PPS) signal. It is not connected to an antenna outside the building but generates satellite signals on its own. The user receives the combined signals from paired transmitters broadcasting identical sets of satellite signals and conducts the signal tracking and positioning. The autocorrelation functions of combined signals are viewed as the overlap of each individual autocorrelation function. Delay-locked-loop (DLL) signal tracking is performed on the overlapping autocorrelation functions. The estimated position can be determined along the track between the two transmitters. Unlike previous studies, the proposed system need not distinguish the signal of each transmitter; nor does it require any additional information such as the location of the transmitters. Therefore, a conventional GNSS receiver can be applied directly. In addition, all of the signals travel the same path from transmitter to receiver, and all are affected by the same multipath. This makes the proposed system robust against multipath error, which is absorbed by the clock bias term in the navigation solution. Leveraging these advantages, it is easy to implement pseudorange-based indoor positioning, which has been difficult to use indoors. We believe that the proposed system makes a significant contribution that has not been achieved in the GNSS-based indoor positioning from the following two perspectives: One is that a commercial GNSS receiver can be used directly, and the other is that the multipath error does not affect position estimation. In addition, we analyze the proposed system theoretically and perform a simulation and field test to verify its validity and feasibility. The remainder of this paper is organized as follows: Section 2 introduces the overview of the proposed system. In particular, we introduce the principle of positioning when two transmitters' signals are combined. Section 3 presents the conducted theoretical analysis to derive the theoretical prompt, pseudorange, and position. Moreover, we explain the reason why the multipath error does not affect the position and analyze the signal power of the proposed system. Section 4 presents the simulation results, through which the theoretical analysis is verified. Section 5 discusses the feasibility of the field test results of the proposed system. Finally, Section 6 presents the conclusions of our study.

2 | SYSTEM OVERVIEW

In this section, we briefly describe the system configuration proposed in this study. We explain the GNSS signal transmitter used in this study and describe the characteristics of the transmitter and the difference from the conventional repeater. Furthermore, we explain the basic concept of the proposed system: When the user receives two transmitters' signals simultaneously, the tracking point of the receiver is described on the overlapping autocorrelation functions.

2.1 | GNSS signal transmitter

A GNSS signal transmitter, which is implemented in the proposed system, plays the same role as a repeater as it broadcasts satellite signals. However, unlike a repeater that relays and broadcasts GNSS signals from an antenna installed outside a building, a transmitter generates and broadcasts GNSS signals corresponding to an arbitrary location. In this study, it is assumed that the transmitter generates GNSS signals that should have been received at the actual transmitter position. A user estimates the position using paired transmitters, which consist of one master transmitter and one slave transmitter. The master exploits ephemeris and time information through the wireless network as well as transmits a PPS signal and ephemeris data to the slave over the wired network. The slave can generate signals synchronized with the master by calibrating the pre-measured line and hardware bias. For more accurate time synchronization with actual GNSS signals, a PPS signal in an outdoor receiver can be used for the master; hence, it is possible to determine the location without a reacquisition process when the user enters an indoor environment from outdoors. In fact, the conventional repeater also can be used in the proposed system, but the transmitter can be applied to environments where it is difficult to install repeaters without (e.g., in tunnels).

2.2 | General concept

Figure 1 shows the indoor environments with two transmitters proposed in this study. Each transmitter is marked with subscript "s1" and "s2." Transmitters are located at \mathbf{R}_{s1} and \mathbf{R}_{s2} , and generate GNSS signals based on their position. Although actual satellite signals cannot be received, for the sake of comprehension, the distance d_{s1}^i and d_{s2}^i between satellite and transmitter are indicated by a dashed line. \mathbf{R}_{sat}^i denotes the i -th PRN satellite position, and \mathbf{R}_u is the user position. l_{s1} and l_{s2} denote the user's distance from transmitters 1 and 2, respectively. Each

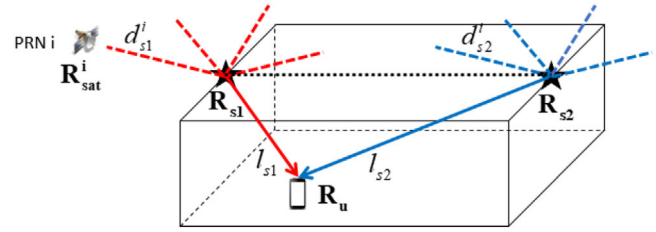


FIGURE 1 Indoor environments with two transmitters (proposed system) [Color figure can be viewed in the online issue, which is available at wileyonlinelibrary.com and www.ion.org]

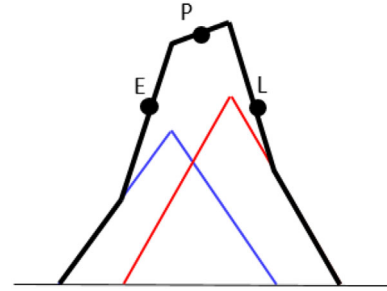


FIGURE 2 Overlapping autocorrelation functions [Color figure can be viewed in the online issue, which is available at wileyonlinelibrary.com and www.ion.org]

transmitter generates simulated GNSS signals corresponding to its position and broadcasts the same set of satellite signals because the transmitters are sufficiently close together. The pseudoranges of each transmitter received by the user are expressed in Equation (1). Here, \mathbf{e}^i indicates the line-of-sight vector of the i -th PRN satellite. All error sources, including hardware delay, are ignored.

$$\begin{aligned}\rho_{s1}^i &= (\mathbf{R}_{sat}^i - \mathbf{R}_{s1}) \cdot \mathbf{e}^i + l_{s1} = d_{s1}^i + l_{s1} \\ \rho_{s2}^i &= (\mathbf{R}_{sat}^i - \mathbf{R}_{s2}) \cdot \mathbf{e}^i + l_{s2} = d_{s2}^i + l_{s2}\end{aligned}\quad (1)$$

If a user receives only the signal of transmitter 1 indicated by a red line, all pseudoranges are l_{s1} common for all channels. A channel is the term separating one PRN signal from all others in the receiver. This term is included in the clock bias in the navigation solution and does not affect the position result. Therefore, the user position is estimated as the transmitter position, \mathbf{R}_{s1} , regardless of the actual user location. However, if a user receives two transmitters' signals at any location, the estimated position is affected by overlapping signal. It is assumed that two transmitters are time synchronized correctly.

The signals broadcast from two transmitters are correlated with the receiver replica signal. Figure 2 shows overlapping autocorrelation functions in the DLL. The autocorrelation function of each transmitter signal has a triangular shape. The height of the triangle is determined

by the signal power, and the offset of two triangles is determined by the pseudorange difference. In the GNSS receiver, signal tracking is conducted at the point where the early and late values are equal in the combined correlation function, as shown by the black line in Figure 2. The prompt value is located between two triangles, which implies that the estimated pseudorange in the receiver is between the two transmitters' pseudoranges. It can be expected that the estimated position will be determined between two transmitters by gathering these estimated pseudoranges. In terms of conventional multipath analysis, engineers have tried to eliminate the reflected signal to retain only the direct signal. In the proposed system, however, the overlapping signals are essential to estimate user position.

3 | THEORETICAL ANALYSIS

In this section, a detailed theoretical analysis of the proposed system is presented. In overlapping autocorrelation functions, as shown in Figure 2, a theoretical prompt component is derived. Subsequently, we derive the pseudorange that the theoretical prompt implies and, thereafter, the user position via the estimated pseudoranges. In addition, analyses of the multipath effect and signal power are introduced.

3.1 | Theoretical prompt

To derive the theoretical prompt, we assume that solely the DLL in the signal tracking loop is considered. The influence of carrier tracking will be discussed in the power analysis. In this study, we make three assumptions for the theoretical analysis: First, the gap between early and late values is one chip, which is the most common value in commercial GNSS receivers. Second, with sufficient control, the theoretical prompt is defined as the value when early and late values are the same. Third, the maximum distance between two transmitters is 0.25 chip (75 m). The distance between two transmitters can be adjusted by the designer, and the value of 75 m is actually reasonable when considering practical application. When the assumptions are satisfied, overlapping autocorrelation functions can be divided into five sections:

1. The section where solely one signal correlates with a positive slope
2. The section where both signals correlate with positive slopes
3. The section where both signals correlate with different signs of slope

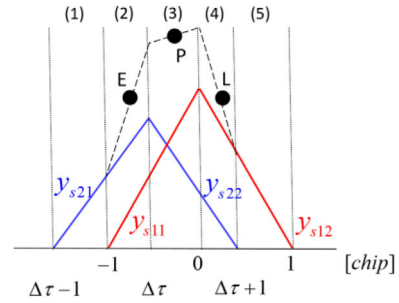


FIGURE 3 Classification of sections according to overlapping [Color figure can be viewed in the online issue, which is available at wileyonlinelibrary.com and www.ion.org]

4. The section where both signals correlate with negative slopes
5. The section where solely one signal correlates with a negative slope

The early and late values continue to exist in sections (2) and (4), respectively, regardless of the difference in signal power ratio and pseudorange (Figure 3). The reason why this happens is described in the appendix.

The functions y_{s11} and y_{s12} , as well as y_{s21} and y_{s22} , represent the correlation results of transmitter 1 and transmitter 2, respectively. If the user is closer to transmitter 1, as shown in Figure 1, the signal power of transmitter 1 is higher than transmitter 2, and the height difference of the triangle indicates this difference. The signal power is inversely proportional to the square of the distance. Therefore, the signal power ratio denoted by α is expressed by Equation (2). The terms A_{s1} and A_{s2} denote the broadcasting signal power in transmitters 1 and 2, respectively. Because all satellite signals are generated by each transmitter, the signal power ratio is the same for all channels.

$$\frac{A_{s1}}{l_{s1}^2} : \frac{A_{s2}}{l_{s2}^2} = 1 : \alpha \quad (2)$$

$$\alpha = \frac{l_{s1}^2 A_{s1}}{l_{s2}^2 A_{s2}}$$

If the receiver replica signal is exactly synchronized with the signal of transmitter 1, the triangle of transmitter 1 is located at zero on the x-axis, as shown in Figure 3. If the pseudorange of transmitter 2 is longer than that of transmitter 1, the triangle of transmitter 2 is located on the left side of the triangle of transmitter 1, and the offset between two triangles denoted by $\Delta\tau$ has a negative value, as shown in Figure 3. Equation (3) depicts the delay of the i -th channel for each transmitter in the above situation. The value τ_r^i represents the delay of the replica signal, and the values τ_{s1}^i and τ_{s2}^i represent the delay of transmitter 1 and

TABLE 1 Autocorrelation function according to sections

Section	Delay range [chip]	Autocorrelation function
(1)	$(\Delta\tau^i - 1, -1)$	y_{s21}
(2)	$(-1, \Delta\tau^i)$	$y_{s21} + y_{s11}$
(3)	$(\Delta\tau^i, 0)$	$y_{s22} + y_{s11}$
(4)	$(0, \Delta\tau^i + 1)$	$y_{s22} + y_{s12}$
(5)	$(\Delta\tau^i + 1, 1)$	y_{s12}

transmitter 2 signals, respectively.

$$\begin{aligned} \Delta\tau_{s1}^i &= \tau_r^i - \tau_{s1}^i = 0 \\ \Delta\tau_{s2}^i &= \tau_r^i - \tau_{s2}^i = \tau_{s1}^i - \tau_{s2}^i \equiv \Delta\tau^i < 0 \end{aligned} \quad (3)$$

The theoretical prompt is determined by two factors: the signal power ratio α and the offset between two autocorrelation functions $\Delta\tau^i$. The absolute signal power is not important because the normalized value is applied when calculating the prompt. The autocorrelation functions for each section are summarized in Equation (4) and Table 1.

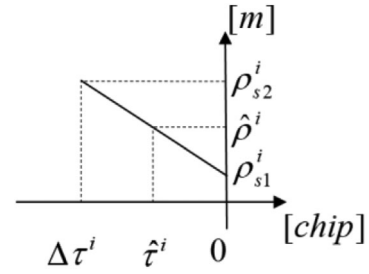
$$\begin{aligned} y_{s11}(x) &= x + 1 \\ y_{s12}(x) &= -x + 1 \\ y_{s21}(x) &= \alpha(x + 1 - \Delta\tau^i) \\ y_{s22}(x) &= \alpha(-x + 1 + \Delta\tau^i) \end{aligned} \quad (4)$$

As mentioned above, the early and late values always exist in sections (2) and (4), regardless of the satellite or user position. The theoretical prompt denoted by $\hat{\tau}^i$, where the early and late values are equal, can be derived as follows:

$$\begin{aligned} &y_{s21}(\hat{\tau}^i - 0.5) + y_{s11}(\hat{\tau}^i - 0.5) \\ &= y_{s22}(\hat{\tau}^i + 0.5) + y_{s12}(\hat{\tau}^i + 0.5) \\ \rightarrow &\alpha(\hat{\tau}^i - 0.5 + 1 - \Delta\tau^i) + (\hat{\tau}^i - 0.5 + 1) \\ &= \alpha(-\hat{\tau}^i - 0.5 + 1 + \Delta\tau^i) + (-\hat{\tau}^i - 0.5 + 1). \quad (5) \\ &(1 + \alpha)\hat{\tau}^i - \alpha\Delta\tau^i = -(1 + \alpha)\hat{\tau}^i + \alpha\Delta\tau^i \\ &(1 + \alpha)\hat{\tau}^i = \alpha\Delta\tau^i \\ \therefore &\hat{\tau}^i = \frac{\alpha}{1 + \alpha}\Delta\tau^i \end{aligned}$$

3.2 | Theoretical pseudorange

The theoretically estimated pseudorange in the receiver can be derived easily exploiting the result of Equation (5). If the prompt value is zero, which is the peak of the autocor-

**FIGURE 4** Relationship between prompt and estimated pseudorange

relation of transmitter 1, the estimated pseudorange will be ρ_{s1}^i . Similarly, if the prompt is on $\Delta\tau^i$, which is the peak of the autocorrelation of transmitter 2, the estimated pseudorange will be ρ_{s2}^i . Figure 4 depicts the relationship between the prompt and the estimated pseudorange.

The theoretical prompt exists between zero and $\Delta\tau^i$, as derived from Equation (5). Therefore, the theoretical pseudorange is expected to exist between two pseudoranges, ρ_{s1}^i and ρ_{s2}^i . The theoretical pseudorange denoted by $\hat{\rho}^i$ can be derived through the simple proportional Equation (6).

$$\begin{aligned} \Delta\tau^i : (\rho_{s2}^i - \rho_{s1}^i) &= \hat{\tau}^i : (\hat{\rho}^i - \rho_{s1}^i) \\ \hat{\rho}^i - \rho_{s1}^i &= \frac{\hat{\tau}^i}{\Delta\tau^i} (\rho_{s2}^i - \rho_{s1}^i) = \frac{\alpha}{1 + \alpha} (\rho_{s2}^i - \rho_{s1}^i) \\ \hat{\rho}^i &= \rho_{s1}^i + \frac{\alpha}{1 + \alpha} (\rho_{s2}^i - \rho_{s1}^i) \\ \therefore \hat{\rho}^i &= \frac{1}{1 + \alpha} \rho_{s1}^i + \frac{\alpha}{1 + \alpha} \rho_{s2}^i \end{aligned} \quad (6)$$

The theoretical pseudorange is expressed as an internally dividing point of the two pseudoranges.

3.3 | Theoretical position

The least squares method is the most common navigation solution algorithm. The theoretical 3D user position $\hat{\mathbf{R}}_{\mathbf{u}}$ and clock bias \hat{b} can be derived through Equation (7). H and \mathbf{z} denote the line-of-sight matrix and the measurement vector, respectively. The superscript m is the total number of satellites.

$$\begin{aligned} \begin{bmatrix} \hat{\mathbf{R}}_{\mathbf{u}} \\ \hat{b} \end{bmatrix} &= (H^T H)^{-1} H^T \mathbf{z} = (H^T H)^{-1} H^T \begin{bmatrix} \mathbf{R}_{\text{sat}}^1 \cdot \mathbf{e}^1 - \hat{\rho}^1 \\ \vdots \\ \mathbf{R}_{\text{sat}}^m \cdot \mathbf{e}^m - \hat{\rho}^m \end{bmatrix} \\ H &= \begin{bmatrix} (\mathbf{e}^1)^T & -1 \\ \vdots & \vdots \\ (\mathbf{e}^m)^T & -1 \end{bmatrix} \end{aligned} \quad (7)$$

The theoretical pseudorange in Equation (6) can be converted to the line-of-sight matrix form.

$$\begin{aligned}
 \hat{\rho}^i &= \frac{1}{1+\alpha} \rho_{s1}^i + \frac{\alpha}{1+\alpha} \rho_{s2}^i \\
 &= \frac{1}{1+\alpha} [(\mathbf{R}_{\text{sat}}^i - \mathbf{R}_{s1}) \cdot \mathbf{e}^i + l_{s1}] \\
 &\quad + \frac{\alpha}{1+\alpha} [(\mathbf{R}_{\text{sat}}^i - \mathbf{R}_{s2}) \cdot \mathbf{e}^i + l_{s2}] \\
 &= \mathbf{R}_{\text{sat}}^i \cdot \mathbf{e}^i - \frac{1}{1+\alpha} \mathbf{R}_{s1} \cdot \mathbf{e}^i - \frac{\alpha}{1+\alpha} \mathbf{R}_{s2} \cdot \mathbf{e}^i + \frac{l_{s1} + \alpha l_{s2}}{1+\alpha} \\
 &= \mathbf{R}_{\text{sat}}^i \cdot \mathbf{e}^i - (\mathbf{e}^i)^T \left[\frac{1}{1+\alpha} \mathbf{R}_{s1} + \frac{\alpha}{1+\alpha} \mathbf{R}_{s2} \right] + \frac{l_{s1} + \alpha l_{s2}}{1+\alpha} \\
 &= \mathbf{R}_{\text{sat}}^i \cdot \mathbf{e}^i - \left[(\mathbf{e}^i)^T \quad -1 \right] \begin{bmatrix} \frac{1}{1+\alpha} \mathbf{R}_{s1} + \frac{\alpha}{1+\alpha} \mathbf{R}_{s2} \\ \frac{l_{s1} + \alpha l_{s2}}{1+\alpha} \end{bmatrix} \quad (8)
 \end{aligned}$$

In Equation (8), the signal power ratio α is independent of the PRN number. By combining Equations (7) and (8), the theoretical user position can be calculated as follows:

$$\begin{aligned}
 \begin{bmatrix} \hat{\mathbf{R}}_u \\ \hat{b} \end{bmatrix} &= (H^T H)^{-1} H^T \mathbf{z} \\
 &= (H^T H)^{-1} H^T H \begin{bmatrix} \frac{1}{1+\alpha} \mathbf{R}_{s1} + \frac{\alpha}{1+\alpha} \mathbf{R}_{s2} \\ \frac{l_{s1} + \alpha l_{s2}}{1+\alpha} \end{bmatrix} \\
 \therefore \begin{bmatrix} \hat{\mathbf{R}}_u \\ \hat{b} \end{bmatrix} &= \begin{bmatrix} \frac{\mathbf{R}_{s1} + \alpha \mathbf{R}_{s2}}{1+\alpha} \\ \frac{l_{s1} + \alpha l_{s2}}{1+\alpha} \end{bmatrix} \quad (9)
 \end{aligned}$$

The theoretical user position is also expressed as an internal dividing form of two transmitters. This is evident because the relationship between pseudoranges and position is linear. The theoretical position is always located on the straight line between two transmitters, as shown by the black dotted line in Figure 1. Therefore, it is impossible to determine the position in the cross and height directions. Conversely, it is possible to determine the position along the track between the two transmitters. If the signal power broadcast by the two transmitters is the same, Equation (9) can be expressed as follows:

$$\begin{aligned}
 \alpha &= \frac{l_{s1}^2}{l_{s2}^2} \quad (\text{when } A_{s1} = A_{s2}) \\
 \begin{bmatrix} \hat{\mathbf{R}}_u \\ \hat{b} \end{bmatrix} &= \begin{bmatrix} \frac{l_{s2}^2 \mathbf{R}_{s1} + l_{s1}^2 \mathbf{R}_{s2}}{l_{s1}^2 + l_{s2}^2} \\ \frac{l_{s1} l_{s2} (l_{s1} + l_{s2})}{l_{s1}^2 + l_{s2}^2} \end{bmatrix} \quad (10)
 \end{aligned}$$

In this case, the theoretical user position is determined exclusively by the distance between the transmitters and user. The last row component in Equations (9) and (10) represents the theoretical clock bias when all error sources are ignored.

3.4 | Influence of multipath

Multipath error is the most challenging issue in indoor positioning. In pseudolite-based indoor positioning, each pseudolite broadcasts a single PRN signal. As the propagation path for each channel varies, the multipath error is different for each channel. Similarly, in conventional repeater-based indoor positioning, which distinguishes the repeater signal by the intentional delay, although each repeater broadcasts all visible satellite signals, it is necessary to distinguish which repeater broadcasts the signals currently received by the user. Because each repeater has a different propagation path, the multipath error affects the navigation solution.

In the proposed system, however, both transmitters broadcast all visible satellite signals with accurate time synchronization. For each transmitter, the propagation paths of all channels are the same; hence, the multipath error of all channels is the same. The effects of multipath error on power are not addressed in this paper. Regarding multipath error in the measurement domain, the pseudoranges of each transmitter are as follows:

$$\begin{aligned}
 \rho_{s1,m}^i &= (\mathbf{R}_{\text{sat}}^i - \mathbf{R}_{s1}) \cdot \mathbf{e}^i + l_{s1} + M_{s1} = \rho_{s1}^i + M_{s1} \\
 \rho_{s2,m}^i &= (\mathbf{R}_{\text{sat}}^i - \mathbf{R}_{s2}) \cdot \mathbf{e}^i + l_{s2} + M_{s2} = \rho_{s2}^i + M_{s2} \quad (11)
 \end{aligned}$$

M_{s1} and M_{s2} represent the multipath errors of transmitters 1 and 2, respectively. The receiver estimates the pseudorange by linearly combining two pseudoranges, as shown in Equation (6).

$$\begin{aligned}
 \hat{\rho}_m^i &= \frac{1}{\alpha + 1} (\rho_{s1}^i + M_{s1}) + \frac{\alpha}{\alpha + 1} (\rho_{s2}^i + M_{s2}) \\
 &= \hat{\rho}^i + \left(\frac{1}{\alpha + 1} M_{s1} + \frac{\alpha}{\alpha + 1} M_{s2} \right) \\
 &= \hat{\rho}^i + B_m \quad (12)
 \end{aligned}$$

The multipath errors cause the same bias, B_m , in all channels. This bias term is absorbed by the clock bias when calculating the navigation solution and does not affect the position estimation. Therefore, as the receiver tracks the combined signals of the two transmitters' signals, the multipath error does not cause bias error in the position estimation.

3.5 | Power analysis

Thus far, the effects of two overlapping signals in the DLL have been analyzed. In addition to DLL, however, carrier tracking is performed in the receiver. In this section, the effect of carrier tracking is presented. The in-phase and quadrature signals of the i -th channel, which are the correlation results with transmitter 1 signal denoted by s_1^i and receiver replica signal denoted by s_r^i , can be modeled as follows (Misra & Enge, 2010):

$$\begin{aligned} s_1^i \otimes s_r^i &= \sqrt{P_{s1}^i} R(\Delta\tau_{s1}^i) \text{sinc}(\pi\Delta f_{D,s1}^i T) \\ &\quad \times \exp(\Delta\phi_{s1}^i + \pi\Delta f_{D,s1}^i T) = C_{s1}^i \exp(\Delta\theta_{s1}^i) \\ &= I_{s1}^i + jQ_{s1}^i, \\ &\quad \left(\begin{array}{l} C_{s1}^i = \sqrt{P_{s1}^i} R(\Delta\tau_{s1}^i) \text{sinc}(\pi\Delta f_{D,s1}^i T) \\ \Delta\theta_{s1}^i = \Delta\phi_{s1}^i + \pi\Delta f_{D,s1}^i T \end{array} \right) \end{aligned} \quad (13)$$

where

$$\begin{aligned} \Delta\tau_{s1}^i &= \hat{\tau}^i - \tau_{s1}^i \\ \Delta f_{D,s1}^i &= \hat{f}_D^i - f_{D,s1}^i \\ \Delta\phi_{s1}^i &= \hat{\phi}^i - \phi_{s1}^i \end{aligned} \quad (14)$$

The noise term is ignored. $R(*)$ is the autocorrelation function, and P is the received signal power. The effects of multipath error on the signal power are not considered. Further, τ, f_D , and ϕ are the code delay, Doppler, and carrier phase, respectively. $\Delta *$ denotes the difference between the estimated value $\hat{*}$ and the replica value $_{s1}$. T denotes the pre-integration time. Because the receiver receives two transmitters' signals, the final in-phase and quadrature values are the sum of each correlation result as follows:

$$\begin{aligned} (s_1^i + s_2^i) \otimes s_r^i &= s_1^i \otimes s_r^i + s_2^i \otimes s_r^i \\ &= (I_{s1}^i + I_{s2}^i) + j(Q_{s1}^i + Q_{s2}^i). \end{aligned} \quad (15)$$

The signal power of two overlapping signals is expressed as follows:

$$\begin{aligned} P^i &= (I_{s1}^i + I_{s2}^i)^2 + (Q_{s1}^i + Q_{s2}^i)^2 \\ &= (C_{s1}^i \cos \Delta\theta_{s1}^i + C_{s2}^i \cos \Delta\theta_{s2}^i)^2 \\ &\quad + (C_{s1}^i \sin \Delta\theta_{s1}^i + C_{s2}^i \sin \Delta\theta_{s2}^i)^2 \\ &= (C_{s1}^i)^2 + (C_{s2}^i)^2 + 2C_{s1}^i C_{s2}^i \cos(\Delta\theta_{s1}^i - \Delta\theta_{s2}^i) \end{aligned} \quad (16)$$

The above result indicates that the overall signal power is not simply the sum of the two transmitters' power, but

the carrier term should be considered. This term occurs inevitably, because two incoming carrier phases should be tracked solely by one replica signal. As the offset on the code domain is represented by two mismatched autocorrelation functions, the offset on the carrier domain is represented by the cosine term of the signal power. In the case of indoor users, the user speed is, generally, not high. Therefore, the phase of cosine in Equation (16), when ignoring the user-induced component of Doppler error, can be expressed as follows:

$$\begin{aligned} \Delta\theta_{s1}^i - \Delta\theta_{s2}^i &= (\Delta\phi_{s1}^i + \pi\Delta f_{D,s1}^i T) - (\Delta\phi_{s2}^i + \pi\Delta f_{D,s2}^i T) \\ &= \left[(\hat{\phi}_{s1}^i - \phi_{s1}^i) + \pi(\hat{f}_D^i - f_{D,s1}^i) \Delta T \right] \\ &\quad - \left[(\hat{\phi}_{s2}^i - \phi_{s2}^i) + \pi(\hat{f}_D^i - f_{D,s2}^i) \Delta T \right] \\ &= (\phi_{s2}^i - \phi_{s1}^i) + \pi(f_{D,s2}^i - f_{D,s1}^i) \Delta T \\ &\approx \phi_{s2}^i - \phi_{s1}^i \end{aligned} \quad (17)$$

where

$$\begin{aligned} \phi_{s1}^i &= (R_{sat}^i - R_{s1}) \cdot e^i + l_{s1} + N_{s1}^i \lambda \\ \phi_{s2}^i &= (R_{sat}^i - R_{s2}) \cdot e^i + l_{s2} + N_{s2}^i \lambda \\ \phi_{s2}^i - \phi_{s1}^i &= (R_{s1} - R_{s2}) \cdot e^i + (l_{s2} - l_{s1}) + (N_{s2}^i - N_{s1}^i) \lambda \\ &= fn(R_{s1}, R_{s2}, e^i, R_u) \end{aligned} \quad (18)$$

Here, N_{s1} and N_{s2} are the integer ambiguities of the transmitters, and λ is the wavelength of GPS L1 signal. The phase of the cosine term can be expressed as the carrier phase difference between two transmitters' signals, which is a function of the transmitter's position, line-of-sight vector, and user position. Because the transmitter location is fixed once installed, the carrier phase difference is actually determined by the user and satellite position. In other words, the signal power has a sine wave shape according to the user's movement. As a special case, if the carrier phase difference is π , the cosine term of Equation (16) has a value of -1. This implies that Equation (16) can be expressed as a perfect square form as follows:

$$\begin{aligned} P^i &= (C_{s1}^i)^2 + (C_{s2}^i)^2 + 2C_{s1}^i C_{s2}^i \cos(\Delta\theta_{s1}^i - \Delta\theta_{s2}^i) \\ &= (C_{s1}^i)^2 + (C_{s2}^i)^2 - 2C_{s1}^i C_{s2}^i \\ &= (C_{s1}^i - C_{s2}^i)^2 \end{aligned} \quad (19)$$

The result of Equation (19) implies that the signal power of the i -th channel can be significantly reduced at a specific user position. This power attenuation occurs whenever the cosine term has a value of -1 in a period of $\lambda = 19$ cm. Fortunately, this phenomenon usually does not occur on

TABLE 2 Settings for signal digitization

Setting	Values
Sampling frequency	5 MHz
Intermediate frequency	2 MHz
Quantization bit	I, Q 16 bit, each

multiple channels simultaneously. Therefore, if more than five satellites are visible, there is no problem in calculating the user position. Since power attenuation is an instantaneous phenomenon, it is not a significant problem for signal tracking in dynamic users; however, it definitely is for static users.

4 | SIMULATION RESULTS

In previous sections, we introduced a new indoor positioning system based on overlapping autocorrelation functions and conducted a theoretical analysis of the proposed system regarding the pseudorange, position, multipath, and power. Here, to verify the analysis, we conduct a simulation and compare the simulation results with the theoretical results.

4.1 | Simulation setting

For simulation, a MATLAB-based intermediate frequency (IF) signal generator and a MATLAB-based post-processing software GNSS receiver developed by the Seoul National University GNSS laboratory are deployed. The process of the IF signal generator is as follows: First, the broadcast ephemeris information corresponding to the entered Coordinated Universal Time (UTC) is loaded. Second, using the satellite position and the entered transmitters' position, an analog signal is generated without considering other error sources. Third, the signal attenuation and signal delay between the two transmitters and the user are calculated. Fourth, analog signals for each transmitter are added, and digitization is conducted according to the settings in Table 2. In this study, we consider GPS L1 signal only.

In the software GNSS receiver, IF data generated by the IF signal generator are employed as input; moreover, signal acquisition, tracking, and navigation calculation are conducted. The signal tracking loop is based on a conventional loop filter, and the least squares method is adopted as the navigation filter. All loop filters are second order, and the DLL, frequency-locked loop, and phased-locked loop have noise bandwidths of 3, 20, and 20 Hz, respectively.

Figure 5 illustrates the simulation environment. Two transmitters are located on the x - z plane, and the distance between the two transmitters is 20 m. The coordinates of

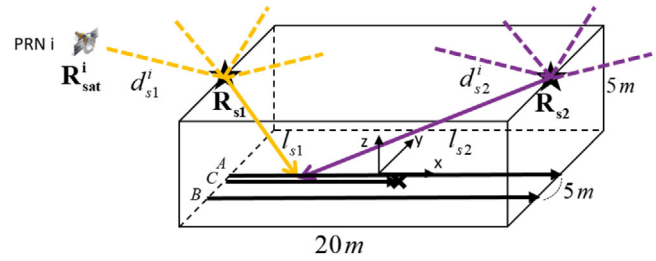


FIGURE 5 Simulation environment [Color figure can be viewed in the online issue, which is available at wileyonlinelibrary.com and www.ion.org]

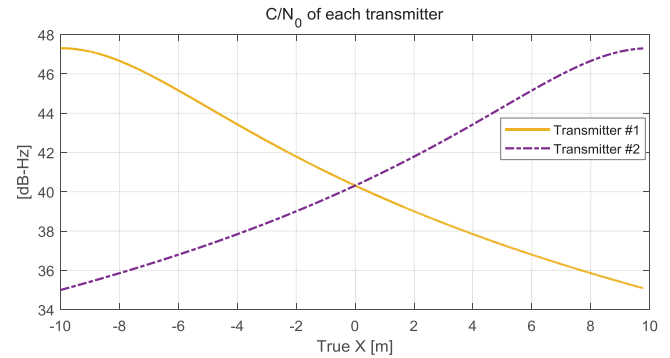


FIGURE 6 Carrier-to-noise power density ratio (C/N_0) values of each transmitter on trajectory A [Color figure can be viewed in the online issue, which is available at wileyonlinelibrary.com and www.ion.org]

the transmitters are $(-10, 0, 5)$ m and $(10, 0, 5)$ m in the East-North-Up (ENU) coordinate frame. The number of visible satellites is eight, and the dilution of precision (DOP) values of both transmitters are 1.78 for position DOP (PDOP), 0.91 for horizontal DOP (HDOP), and 1.53 for vertical DOP (VDOP). Both transmitters broadcast with the same signal strength, and all the effects of signal strength other than signal attenuation according to the distance between transmitters and user are ignored. The height between transmitters and user is 5 m, and three trajectories A–C are implemented for the simulation. Each trajectory is shown in Figure 5 and thoroughly described in the following subsection.

4.2 | Dynamic user

First, a simulation is performed when the user moves at a constant speed of 2 m/s. The user on trajectory A is moving on the x -axis for 10 s, and the user on trajectory B is moving on $y = -5$. Given enough time before the departure, the user starts moving when the navigation solution can be calculated immediately.

Figure 6 shows the carrier-to-noise power density ratio (C/N_0) values of each transmitter signal when the user

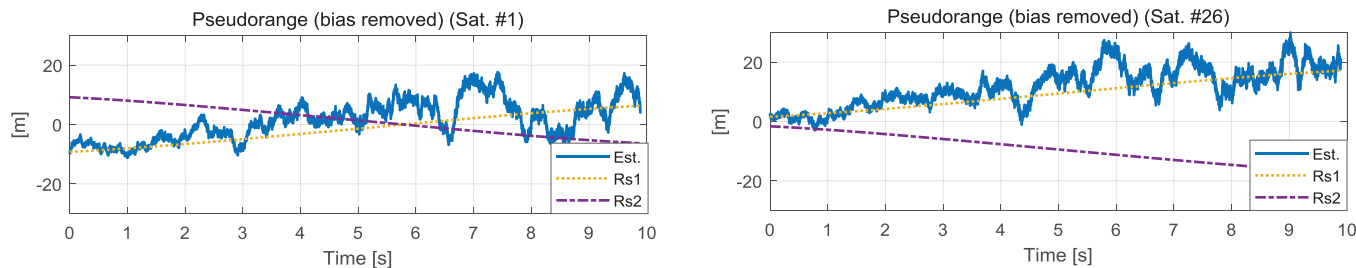


FIGURE 7 Pseudorange estimation results when only transmitter 1 is enabled: estimated pseudorange (blue), pseudorange of transmitter 1 (yellow), and pseudorange of transmitter 2 (purple) [Color figure can be viewed in the online issue, which is available at wileyonlinelibrary.com and www.ion.org]

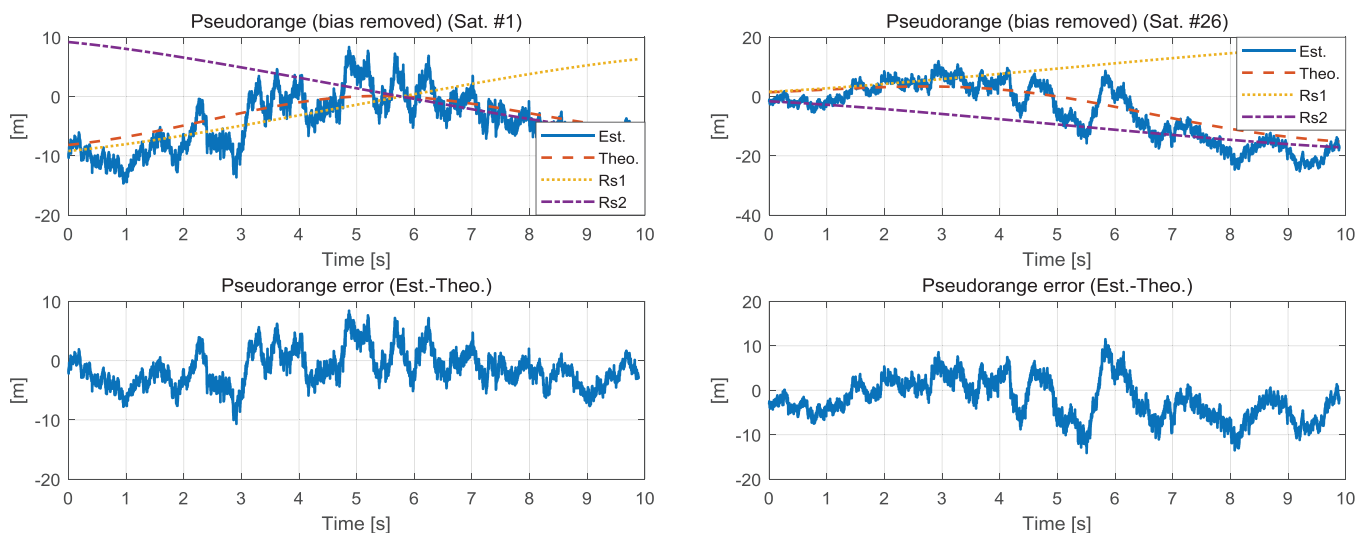


FIGURE 8 Pseudorange estimation results when paired transmitters are enabled: estimated pseudorange (blue), theoretical pseudorange (red), pseudorange of transmitter 1 (yellow), and pseudorange of transmitter 2 (purple) [Color figure can be viewed in the online issue, which is available at wileyonlinelibrary.com and www.ion.org]

moves on trajectory A. The C/N_0 values range from 35.1 to 47.3 dB-Hz depending on the user’s location.

Figure 7 shows the results of the estimated pseudorange of two channels of the eight visible satellites when only transmitter 1 is enabled. The level of the pseudorange measurements is adjusted to focus on the pseudorange deviation according to the dynamic user. The results show that the estimated pseudorange follows the pseudorange of transmitter 1 with noise. Because the C/N_0 of transmitter 1 decreases to 35 dB-Hz to 39 dB-Hz after 6 s, the pseudorange estimation error can increase.

Figure 8 shows the results of the estimated pseudoranges when paired transmitters are enabled. The theoretical pseudorange is expressed as the internal division form between the two transmitters’ pseudoranges, as expressed in Equation (6). The estimated pseudorange has the same trend as the theoretical results, but it appears to have large errors, especially from 4 s to 6 s. The minimum combined

signal power in the receiver can be expressed as the difference between the signal power of each transmitter. Therefore, at the midpoint where the signal powers of two transmitters are similar, the combined signal power can momentarily drop to near zero. This power instability can instantaneously cause a large error in DLL. A detailed description of the power analysis can be found in Subsection 4.4.

Figure 9 depicts the East and North of the ENU coordinate frame estimation results. The theoretical position is the internally dividing point of two transmitters, as expressed in Equation (9), and it is confirmed that the user can be determined in the East direction, that is, along the track between transmitters. The North and up position estimation should be calculated as 0 and 5, because the North and up of both transmitters are 0 and 5, respectively. Table 3 shows the statistical values of the pseudorange and position error. The values related to pseudorange are the

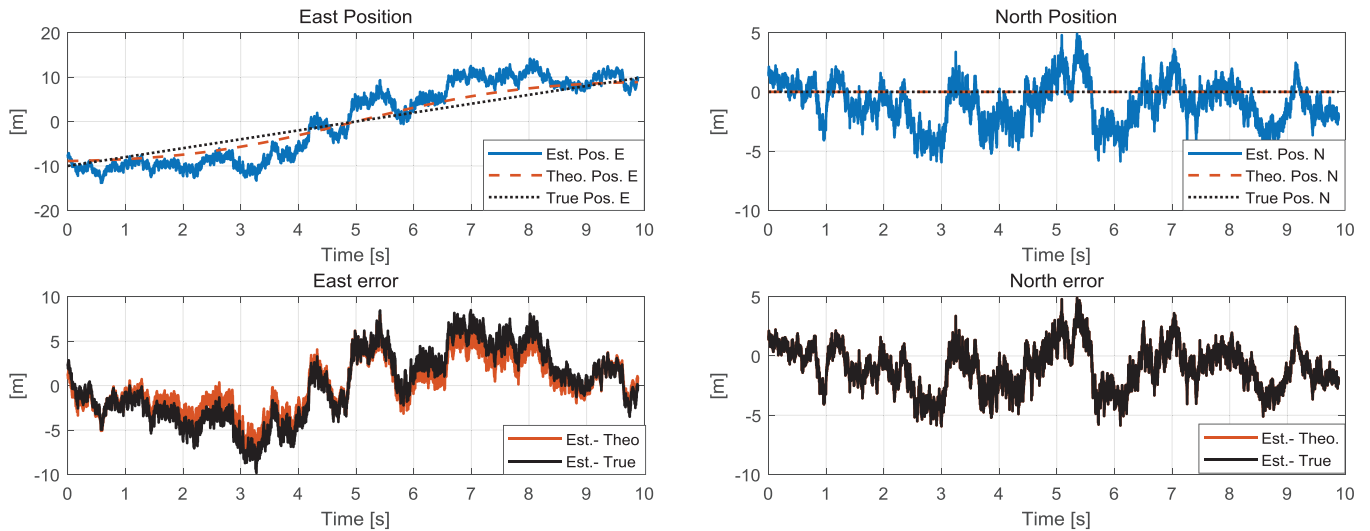


FIGURE 9 Position estimation results when the user moves on trajectory A: estimated position (blue), theoretical position (red), and true position (black) in the upper graphs, and the estimated position error versus theoretical position (red), and true position (black) in the lower graphs [Color figure can be viewed in the online issue, which is available at wileyonlinelibrary.com and www.ion.org]

TABLE 3 Standard deviation (STD), bias, and root-mean-square (RMS) values of pseudorange and position error in the case of trajectory A

		STD [m]	Bias [m]	RMS [m]
Pseudorange error (vs. Theoretical)		3.95	1.57	4.28
Position error (vs. Theoretical)	East	2.95	0.03	2.95
	North	1.83	1.00	2.08
	Up	6.10	1.76	6.35
Position error (vs. True)	East	3.87	0.04	3.87
	North	1.83	1.00	2.08
	Up	6.11	6.77	9.11

average values of all channels. We can confirm that the proposed system can estimate the user position within 4 m of root-mean-square (RMS) error in the East direction.

Subsequently, a simulation is conducted when the user moves at a speed of 2 m/s from (-10, -5, 0) m to (10, -5, 0) m on trajectory B. In this case, the C/N_0 values of each transmitter’s signal range from 34.8 dB-Hz to 44.3 dB-Hz depending on user location. Compared to trajectory A, a slight decrease in C/N_0 occurs because the distance between transmitters and user increases. However, since the position estimation is performed using the C/N_0 ratio of the two transmitters, this absolute signal strength reduction does not influence the East position estimation. Figure 10 shows the East and North position estimation results.

We can confirm that the East position can be estimated, as in the case of trajectory A; that is, the bias error of 5 m occurs in the estimation of the North position. These

results imply that the proposed system cannot determine the position in the cross direction, perpendicular to the track. Conversely, the position estimation of the up direction has a bias error of 5 m, because the height of the transmitters is 5 m. Table 4 shows the statistic values of the pseudorange and position error in the case of trajectory B. Similar to the previous result, the proposed system can estimate the user position with RMS error of about 3 m in the East direction.

4.3 | Influence of multipath error

A simulation is conducted to determine the influence of the multipath error analyzed in Subsection 3.4. The user moves on trajectory A, and sine wave multipath errors are added to each transmitter, as shown in Figure 11. The multipath errors affect all visible satellite measurements generated by each transmitter.

As shown in Equation (12), the multipath error causes a common bias term, B_m . This term is additional to the theoretical bias term in Equation (9) in the absence of multipath error. The red dashed line on the clock bias graph in Figure 12 represents the theoretical clock bias, in which the effects of multipath errors are considered. The clock bias estimated through the simulation tends to be the same as the theoretical result. Therefore, it is confirmed that the East position estimation is possible regardless of the multipath error. Moreover, the positioning in the other direction has the same tendency as when no multipath error exists. The East position error is similar to Table 3 and 4 results, with RMS errors of 3.50 m.

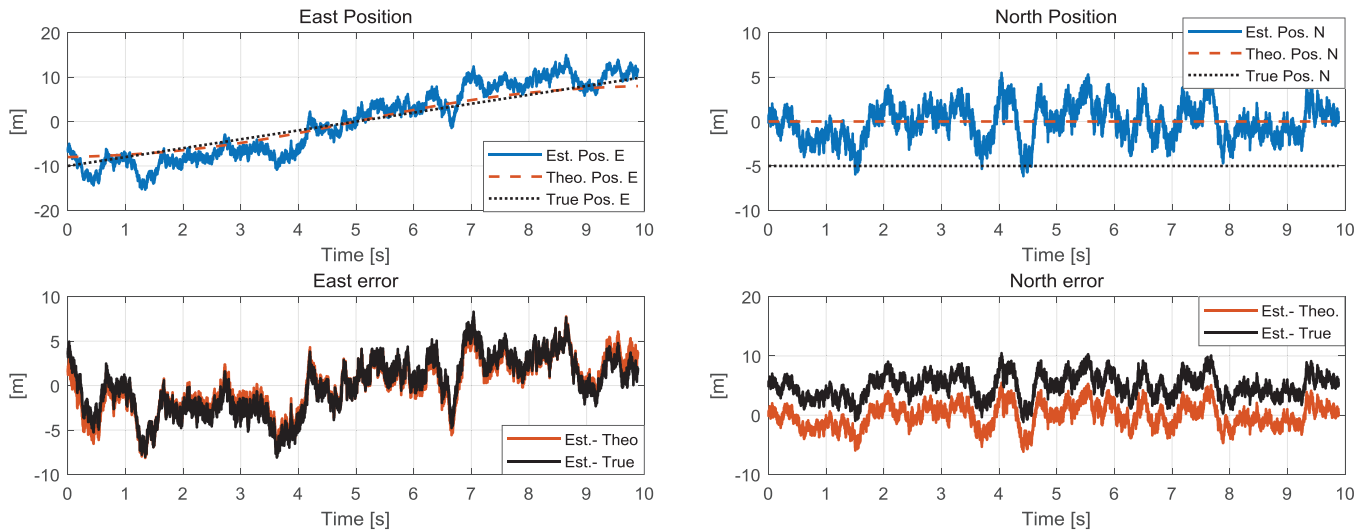


FIGURE 10 Position estimation results when the user moves on trajectory B: estimated position (blue), theoretical position (red), and true position (black) in the upper graphs; the estimated position error versus theoretical position (red), and true position (black) in the lower graphs [Color figure can be viewed in the online issue, which is available at wileyonlinelibrary.com and www.ion.org]

TABLE 4 STD, bias, and RMS values of pseudorange and position error in the case of trajectory B

		STD [m]	Bias [m]	RMS [m]
Pseudorange error (vs. Theoretical)		4.17	1.05	4.30
Position error (vs. Theoretical)	East	2.95	0.01	2.95
	North	1.97	0.08	1.97
	Up	6.03	0.11	6.03
Position error (vs. True)	East	3.09	0.00	3.09
	North	1.97	4.92	5.30
	Up	6.03	5.12	7.97

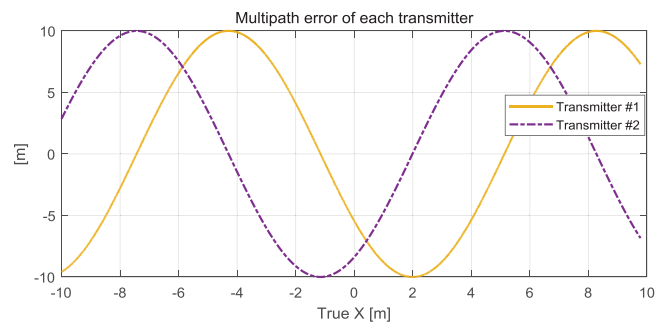


FIGURE 11 Multipath error of each transmitter [Color figure can be viewed in the online issue, which is available at wileyonlinelibrary.com and www.ion.org]

4.4 | Power analysis simulation

To analyze the signal power of the proposed system, a simulation is conducted on trajectory C. The user starts at a speed of 2 m/s at (-10, 0, 0) m and stops at (0.132, 0, 0) m. The latter is the point at which the difference of carrier phase measurements of PRN #1 broadcast by the two transmitters is exactly π . As expressed in Equation (19), the signal power of PRN #1 is expressed in the form of a perfect square of the difference between signal strengths of the two transmitters. In particular, because 0.132 m corresponds approximately to the middle point between the two transmitters, the signal power difference is almost zero. Therefore, the signal power of PRN #1 is expected to be very low. In contrast, the signal power of other channels is adequate enough to calculate the position. Figures 13 and 14 depict the received signal power and the C/N_0 estimated by the

receiver of PRN #1 and #26, respectively. Figure 13 shows that the signal power of PRN #1 is expressed in a sine wave, as shown in Equation (16), and is significantly reduced in the static region. The C/N_0 value does not oscillate compared to the signal power because C/N_0 is estimated by the filtering process in the receiver. Figure 14 shows that the signal power of PRN #26 remains high in the static region because the difference of carrier phase measurements of PRN #26 is far from π .

Figure 15 presents the results of the estimated pseudoranges of PRN #1 and #26. The C/N_0 of PRN #1 is reduced to 35 dB-/Hz in static; the RMS error of pseudorange is 7.35 m. In contrast, the C/N_0 of PRN #26 is constantly 43 dB-/Hz in static; the RMS error of pseudorange is 3.89 m, which is half of the result of PRN #1. These results imply that it could be difficult to track a certain PRN signal according to the position where the differenced carrier phase

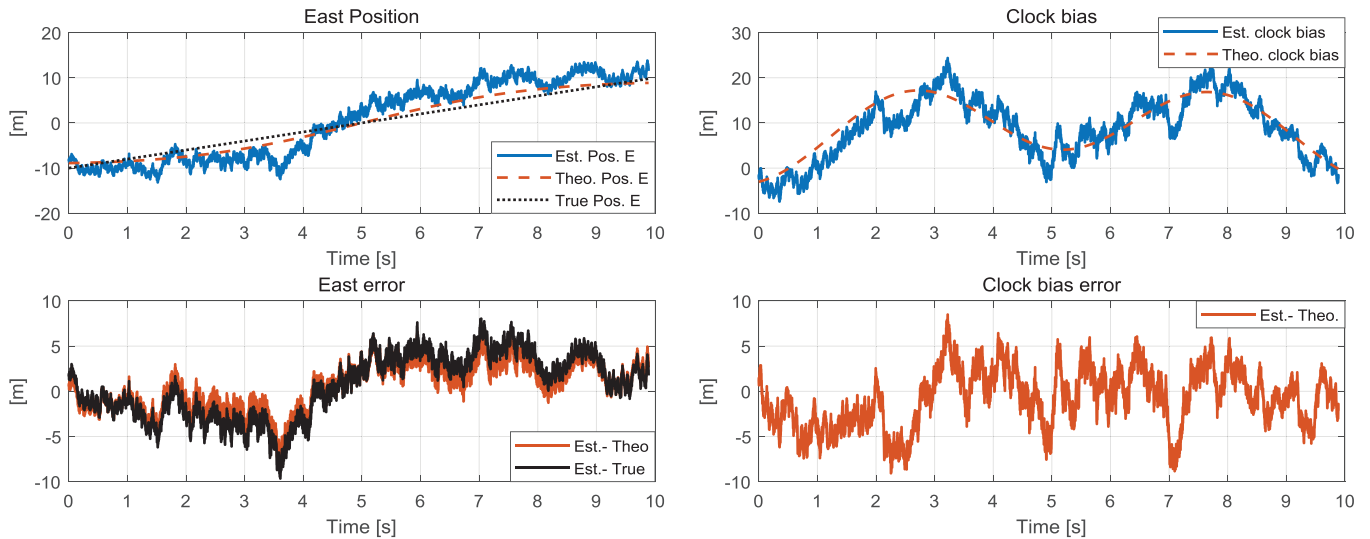


FIGURE 12 East position and clock bias estimation when there is a multipath error: estimation values (blue), theoretical values (red), and true value (black) in the upper graphs; the estimated position error versus theoretical position (red), and true position (black) in the lower graphs [Color figure can be viewed in the online issue, which is available at wileyonlinelibrary.com and www.ion.org]

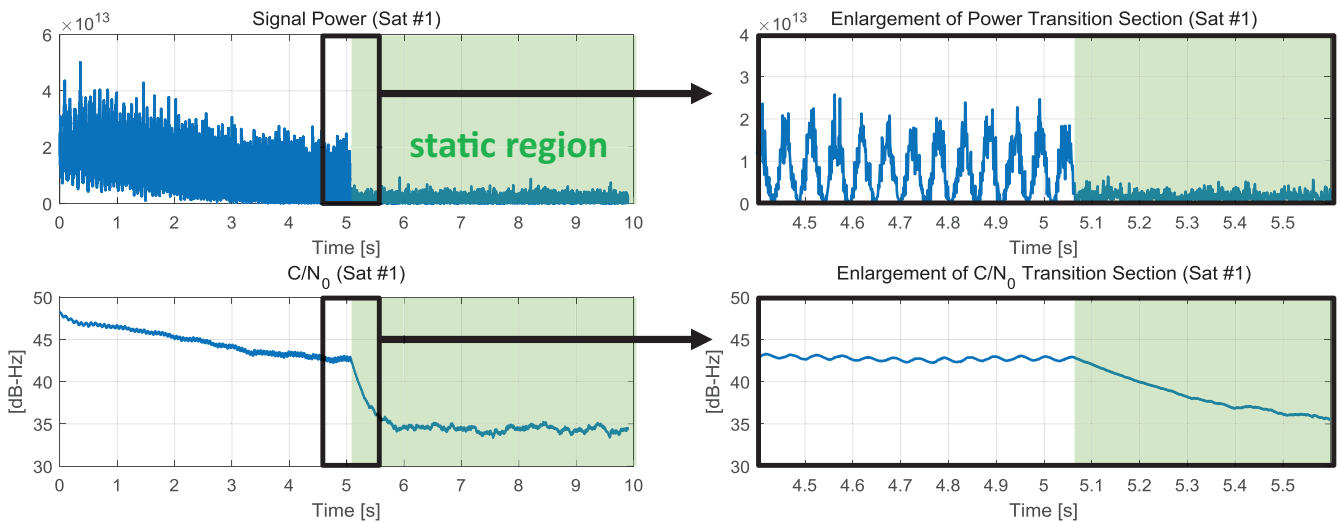


FIGURE 13 Signal power and C/N_0 of pseudorandom noise (PRN) #1 (left). Section that changes from dynamic to static (right) [Color figure can be viewed in the online issue, which is available at wileyonlinelibrary.com and www.ion.org]

measurement is a multiplier of π . However, since the C/N_0 values of multiple satellites rarely decrease simultaneously, there is no problem in estimating the position if the visible satellites are sufficient.

5 | FIELD TEST RESULTS

The field test of the proposed system was designed to test feasibility rather than practicality. The test was conducted by deploying 30 transmitters installed in an underground shopping center of Sogong-dong, Republic of Korea,

located at 126.98 degrees East longitude and 37.56 degrees North latitude, as shown in Figure 16. The transmitters are installed approximately 10 m apart and broadcast GPS signals with a signal power ranging from -105 to -95 dBm. The transmitters consist of one master and 29 slaves, and time synchronization has been achieved based on the master transmitter. A user walking upright under the transmitters receives signals from 25 to 45 dB-Hz depending on their position. The height of the transmitter is approximately 1.3 m above the head of the user. The right upper graph of Figure 16 shows the signal range of each transmitter. For the theoretical analysis, we assumed that indoor users

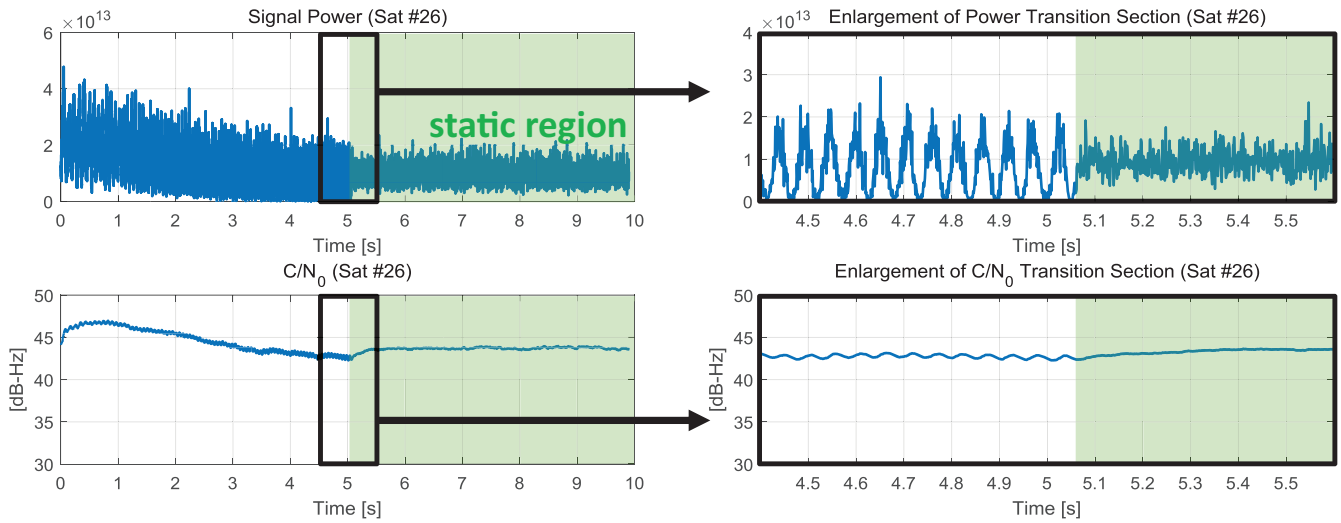


FIGURE 14 Signal power and C/N_0 of PRN #26 (left). Section that changes from dynamic to static (right) [Color figure can be viewed in the online issue, which is available at wileyonlinelibrary.com and www.ion.org]

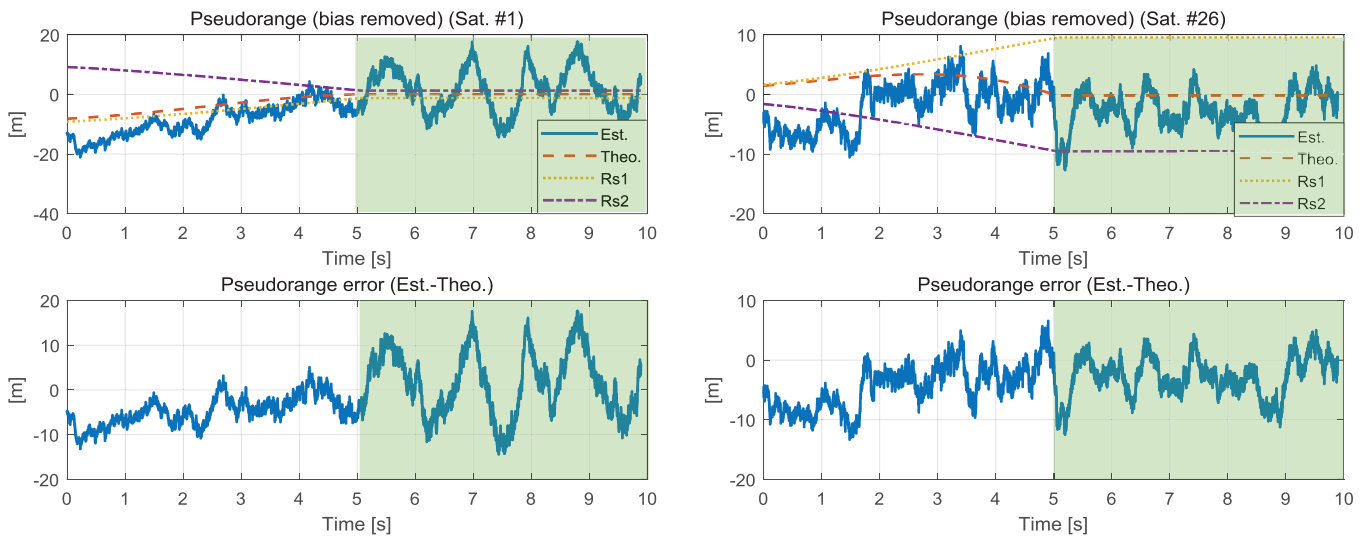


FIGURE 15 Pseudorange estimation results: estimated pseudorange (blue), theoretical pseudorange (red), pseudorange of transmitter 1 (yellow), and pseudorange of transmitter 2 (purple) [Color figure can be viewed in the online issue, which is available at wileyonlinelibrary.com and www.ion.org]

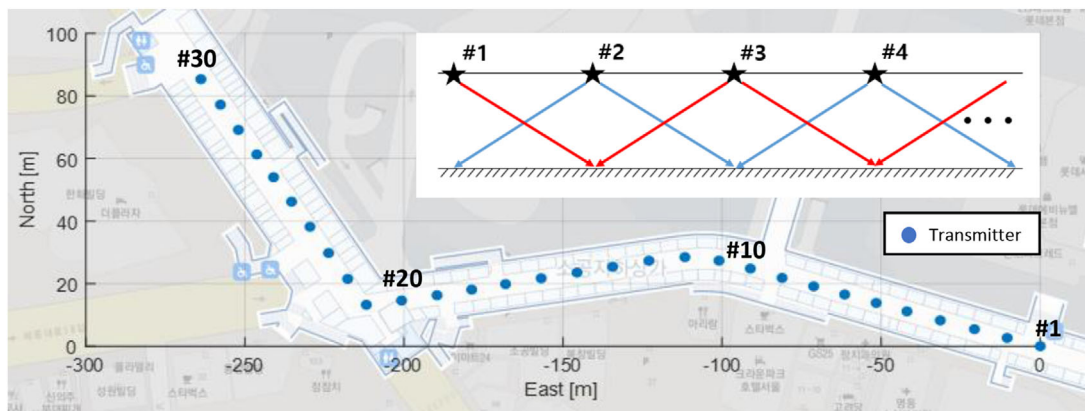


FIGURE 16 Transmitters' position and signal range (upper right) installed in an underground shopping center [Color figure can be viewed in the online issue, which is available at wileyonlinelibrary.com and www.ion.org]



FIGURE 17 Field test setting [Color figure can be viewed in the online issue, which is available at wileyonlinelibrary.com and www.ion.org]

always receive only two adjacent transmitter signals. In reality, more than three transmitter signals can be received depending on the power tuning. However, because the signal power of the additional transmitter signal is much lower than that of the two adjacent transmitter signals, only the effect of these two transmitters is considered. With proper transmitter signal power and antenna pattern, the user always receives only two transmitters' signals. All transmitters are connected in line for time synchronization. The ionosphere and troposphere delay errors are generated in transmitters for each channel using the Klobuchar model (Kaplan & Hegarty, 2017) and the Wide Area Augmentation System model (RTCA SC-159, 2006). The conventional receiver removes these errors from measurement before navigation; therefore, these intentional errors must be added to the transmitter signals.

In the field test in July 2020, transmitter #21 was broken and the signal was not properly broadcast. However, it was not a critical problem in determining the feasibility of the proposed system. A low-cost u-blox 6T receiver and a Samsung Galaxy S20 smartphone were used. We walked exactly under transmitters at a speed of approximately 1 m/s. The patch antenna connected to the u-blox receiver was attached to the hat, and the smartphone was held by a pedestrian, as shown in Figure 17. The number of visible satellites was nine, and the DOP values were 1.51 for PDOP, 0.84 for HDOP, and 1.26 for VDOP.

Figure 18 shows the C/N_0 values of all channels in field tests. When a user passed right underneath the transmitters, the received C/N_0 values were approximately 45 dB-Hz. However, when located at the midpoint between transmitters, the received C/N_0 values drop to 30 dB-Hz, and, in severe cases, below 25 dB-Hz. Figures 19 and 20 show the estimation results of the horizontal position and East and North position respectively. The result of the Galaxy S20 was the position calculated in the Android operating system by itself. In the case of u-blox 6T, the post-processed least squares position was exploited using raw measurements. The reason for the significant increase of the position at GPS time of $1.95 \cdot 10^5$ s is that the user passed under broken transmitter #21. The true position is obtained by checking the passing time exactly under each transmitter with a video camera. It is confirmed that both the smartphone and u-blox results follow a true trajectory on average.

Table 5 presents the statistic values of position error. The horizontal RMS errors of u-blox 6T and Galaxy S20 are approximately 4 m and 7 m, respectively. The reason why the RMS errors are quite large is the influence of the low C/N_0 . By adjusting the transmit signal power in the transmitter, the navigation performance can be improved. However, the current result implies that the proposed system can determine the position along the track on which transmitters are installed. It also implies that commercial smartphones and low-cost GNSS receivers can be used immediately.

For better position estimation, we developed an extended Kalman filter (EKF)-based navigation filter suitable for the proposed system. The EKF uses the pseudorange and the Doppler as measurements. However, the Doppler measurements cannot properly reflect the user dynamic in the proposed system, and only the pseudorange measurements are usefully used to estimate user position. Therefore, the weighting of the pseudorange in the measurement covariance matrix is set much higher than that of the Doppler. Further, we conducted a test using a Samsung Galaxy S10. By developing a GPS logger application, the position using the EKF can be logged in real time. When the user walked back and forth exactly under transmitters, all transmitters operated normally.

Figure 21 shows the horizontal position result of the Galaxy S10. The blue dot represents the position calculated by the device itself, and the red dot represents the position derived from the EKF developed by the authors. The position performance of the S10 is worse than that of the S20. Because different navigation filters are applied for each model, the position performance can be different for each model. However, after the filtering process is made suitable for the proposed system, the horizontal and vertical RMS

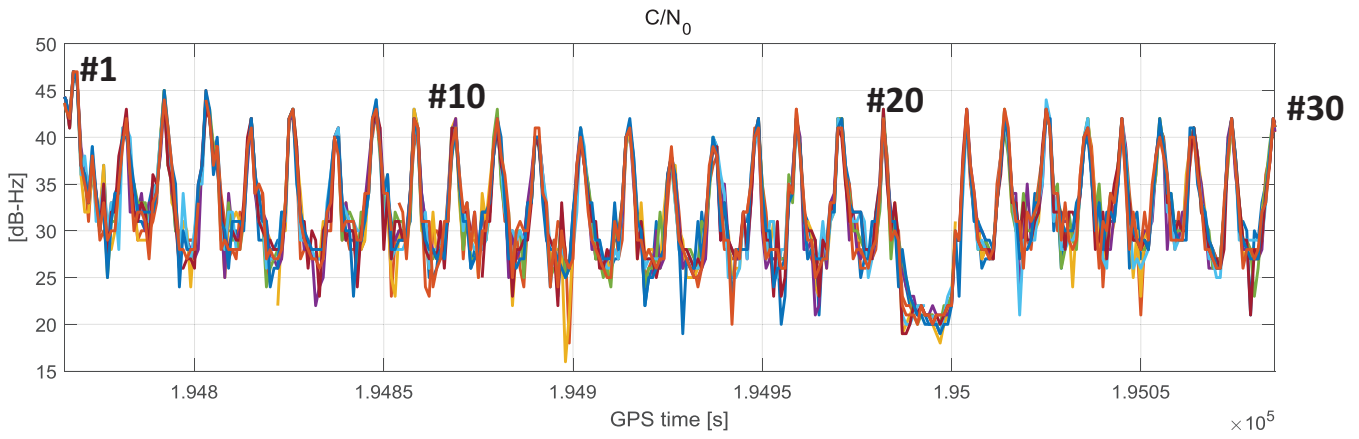


FIGURE 18 C/N_0 values of all channels [Color figure can be viewed in the online issue, which is available at wileyonlinelibrary.com and www.ion.org]

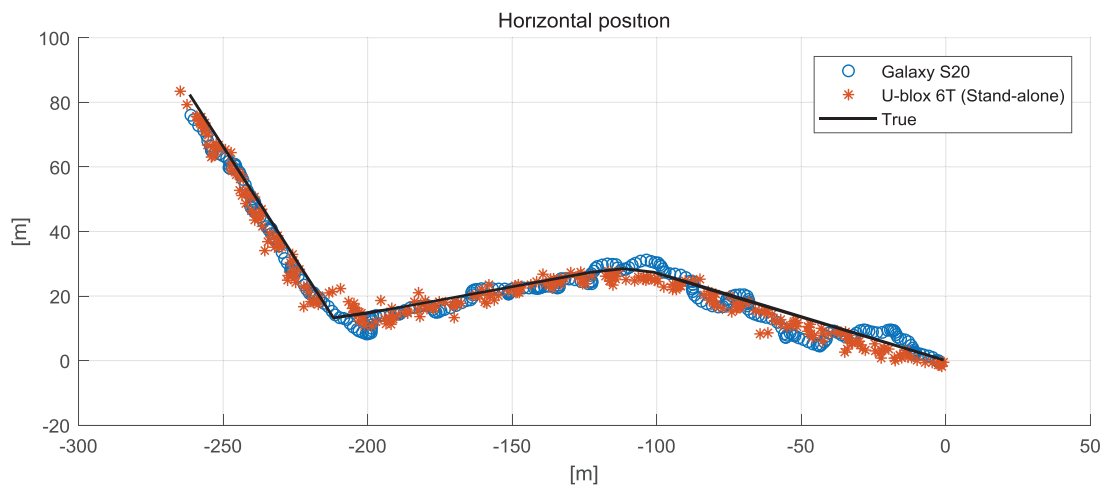


FIGURE 19 Horizontal position results: Galaxy S20 (blue), u-blox 6T (red), and true position (black) [Color figure can be viewed in the online issue, which is available at wileyonlinelibrary.com and www.ion.org]

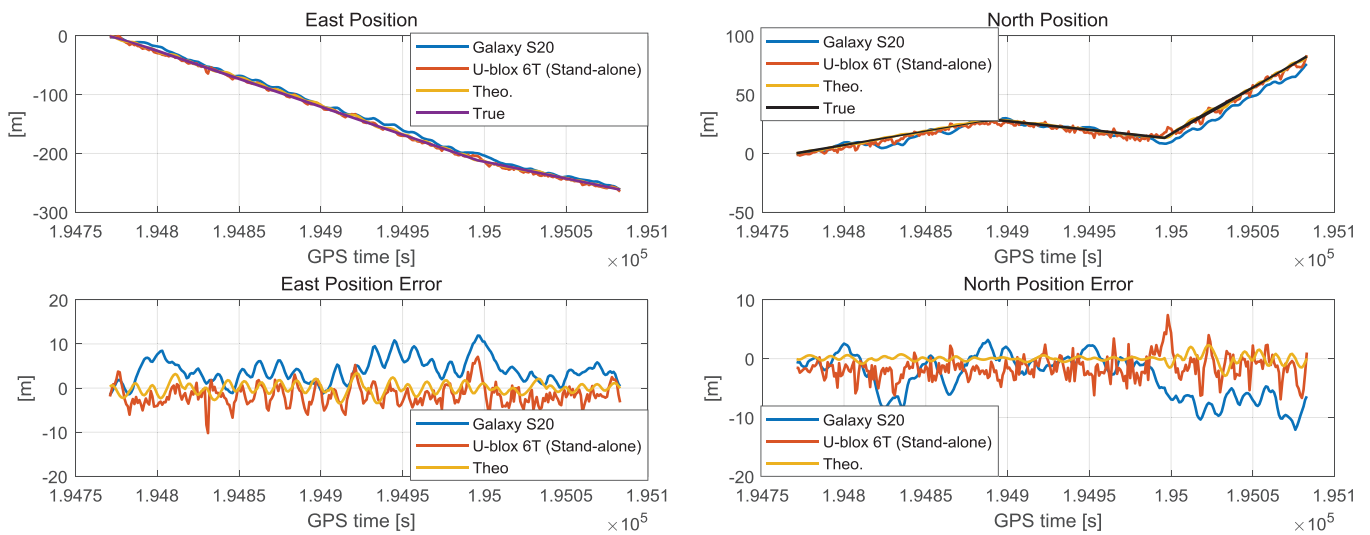


FIGURE 20 East and North position estimation results: Galaxy S20 (blue), u-blox 6T (red), theoretical position (yellow), and true position (black) [Color figure can be viewed in the online issue, which is available at wileyonlinelibrary.com and www.ion.org]

TABLE 5 STD, bias, and RMS values of position error of u-blox and smartphone

		STD [m]	Bias [m]	RMS [m]
U-blox 6T, stand-alone	Horizontal	3.12	2.21	3.83
Position error (vs. True)	Up	3.69	3.52	5.10
Samsung Galaxy S20,	Horizontal	4.29	5.06	6.83
Position error (vs. True)	Up	2.71	4.42	5.19

errors of the S10 will be approximately 3.50 m and 1.82 m, respectively. Therefore, the position performance of smartphones can be improved through an additional navigation filter even if the position results of the smartphone itself are not robust.

6 | CONCLUSIONS

This study proposes a new indoor positioning system based on paired transmitters. This system enables one-way navigation along the track between two transmitters and has the advantage that the commercial GNSS receiver can be used directly, without additional navigation filters. In addition, the system is very robust against multipath error, the biggest problem of pseudorange-based indoor positioning. The proposed system is expected to be widely employed in places with limited movement, such as tunnels and indoor parking lots.

In this system, the theoretical prompt is estimated as the value between the peaks of the two autocorrelation functions. The theoretical pseudorange and position are expressed as an internal division form between two

transmitters' pseudoranges and positions. The simulation results indicate that along track positioning is possible with an RMS error of 4 m. In the simulation, there is a bias error of 5 m in the up direction, which always exists because the reference position of the generating signal in the transmitter is the actual transmitter's position with a bias of 5 m. If the reference position of the generating signal is adjusted to the position of an indoor user, the bias level in the up direction can be significantly reduced. In addition, we confirm that all channels have the same multipath error, which is absorbed by the clock bias term and does not cause the bias error in the position estimation. In the theoretical analysis of the signal power, we confirm that the signal power has a sine wave form according to the carrier phase difference between two transmitters. This implies that the signal tracking of a particular satellite can sometimes be difficult for a static user.

The feasibility test of the proposed system was performed by deploying 30 transmitters in indoor shopping centers. We confirm that both the low-cost receiver and smartphone can be positioned directly when applying the proposed system. The u-blox receiver can estimate the position with an RMS error of 4 m in the horizontal direction. The horizontal RMS error of the smartphone is also within 4 m when using the EKF-based navigation filter.

However, the proposed system can only determine the position along the track between two transmitters. In the future, a study for cross-track positioning will be conducted. In addition, based on the theoretical analysis in this paper, the optimal transmitter arrangement according to height as well as the influence of time synchronization error between transmitters will be investigated.

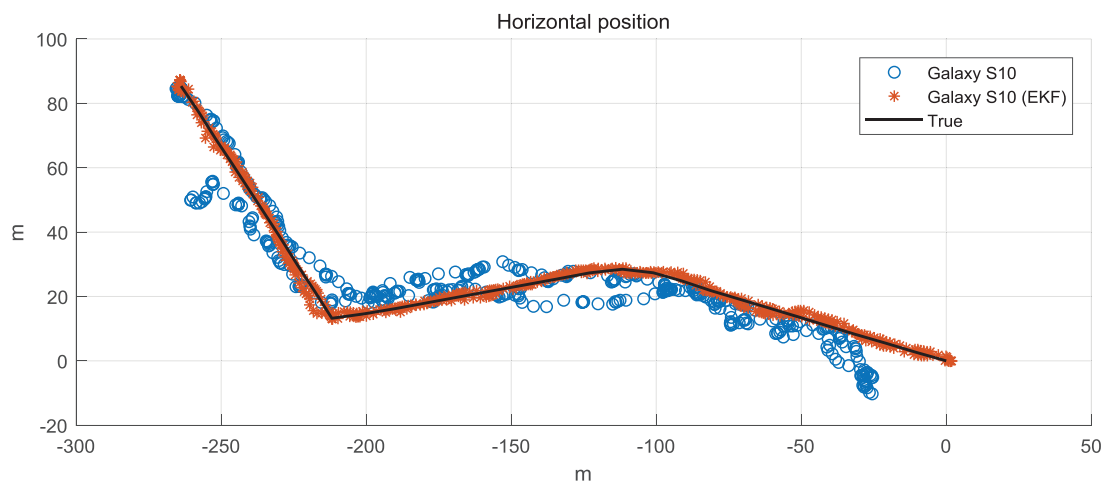


FIGURE 21 Horizontal position results: Galaxy S10 (blue), Galaxy S10 with extended Kalman filter (red), and true position (black) [Color figure can be viewed in the online issue, which is available at wileyonlinelibrary.com and www.ion.org]

ACKNOWLEDGMENTS

This research was supported by Unmanned Vehicles Core Technology Research and Development Program through the National Research Foundation of Korea (NRF), Unmanned Vehicle Advanced Research Center (UVARC), funded by the Ministry of Science and ICT, the Republic of Korea, contracted through by SNU Future Innovation Institute. This research was supported (in part) by the Institute of Advanced Aerospace Technology at Seoul National University. The Institute of Engineering Research at Seoul National University provided research facilities for this work.

ORCID

Minhuck Park  <https://orcid.org/0000-0001-5016-0115>

O-Jong Kim  <https://orcid.org/0000-0003-0752-6219>

Jungbeom Kim  <https://orcid.org/0000-0003-0532-1172>

REFERENCES

- Abdallah, A. A., Shamaei, K., & Kassas, Z. M. (2019). Indoor localization with LTE carrier phase measurements and synthetic aperture antenna array. *Proc. of the 32nd International Technical Meeting of the Satellite Division of the Institute of Navigation (ION GNSS+ 2019)*, Miami, FL, 2670–2679. <https://doi.org/10.33012/2019.17030>
- Ai, H., Zhang, S., Tang, K., Li, N., Huang, W., & Wang, Y. (2019). Robust low-latency indoor localization using Bluetooth low energy. *Proc. of the ION 2019 Pacific PNT Meeting*, Honolulu, HI, 58–72. <https://doi.org/10.33012/2019.16793>
- Im, S. H., Jee, G. I., & Cho, Y. B. (2006). An indoor positioning system using time-delayed GPS repeater. *Proc. of the 19th International Technical Meeting of the Satellite Division of the Institute of Navigation (ION GNSS 2006)*, Fort Worth, TX, 2478–2483.
- Jardak, N. & Samama, N. (2009). Indoor positioning based on GPS-repeaters: Performance enhancement using an open code loop architecture. *IEEE Trans. on Aerospace and Electronic Systems*, 45(1), 347–359. <https://doi.org/10.1109/TAES.2009.4805284>
- Jee, G.-I., Choi, J.-H., & Bu, S.-C. (2004). Indoor positioning using TDOA measurements from switching GPS repeater. *Proc. of the 17th International Technical Meeting of the Satellite Division of the Institute of Navigation (ION GNSS 2004)*, Long Beach, CA, 1970–1976.
- Jee, G.-I., Lee, J.-H., & Im, S.-H. (2005). Indoor positioning using time synchronized switching GPS repeater. *Proc. of the 18th International Technical Meeting of the Satellite Division of the Institute of Navigation (ION GNSS 2005)*, Long Beach, CA, 2769–2774.
- Kaplan, E. D. & Hegarty, C. J. (Eds.). (2017). *Understanding GPS/GNSS: Principles and Applications* (3rd ed.). Artech House.
- Kee, C., Jun, H., & Yun, D. (2003). Indoor navigation system using asynchronous pseudolites. *Journal of Navigation*, 56(3), 443–455. <https://doi.org/10.1017/S0373463303002467>
- Kim, O.-J. & Kee, C. (2019). Single station-based precise positioning system: Multiple-antenna arrangement for instantaneous ambiguity resolution. *NAVIGATION*, 66(4), 747–768. <https://doi.org/10.1002/navi.329>
- Kim, O.-J., Shin, B., Kee, C., Kim, C., Lee, T., So, H., & Kim, G. (2019). Single transmitter based precise positioning system using multiple antenna: Experimental test. *Proc. of the 2019 International Technical Meeting of the Institute of Navigation*, Reston, VA, 446–458. <https://doi.org/10.33012/2019.16703>
- Kok, M., Hol, J. D., & Schön, T. B. (2015). Indoor positioning using ultrawideband and inertial measurements. *IEEE Trans. on Vehicular Technology*, 64(4), 1293–1303. <https://doi.org/10.1109/TVT.2015.2396640>
- Lachapelle, G. (2004). GNSS indoor location technologies. *Journal of Global Positioning Systems*, 3(1&2), 2–11.
- Landa, V., Ben-Moshe, B., Hacothen, S., & Shvalb, N. (2019). GoIn—An accurate 3D indoor navigation framework based on light landmarks. *NAVIGATION*, 66(3), 633–642. <https://doi.org/10.1002/navi.326>
- Li, X. (2019). A GPS-based indoor positioning system with delayed repeaters. *IEEE Trans. on Vehicular Technology*, 68(2), 1688–1701. <https://doi.org/10.1109/TVT.2018.2889928>
- Mautz, R. (2012). *Indoor positioning technologies*. [Habilitation thesis, ETH Zurich, Department of Civil, Environmental and Geomatic Engineering, Institute of Geodesy and Photogrammetry]. <https://doi.org/10.3929/ethz-a-007313554>
- Mazuelas, S., Bahillo, A., Lorenzo, R. M., Fernandez, P., Lago, F. A., Garcia, E., Blas, J., & Abril, E. J. (2009). Robust indoor positioning provided by real-time RSSI values in unmodified WLAN networks. *IEEE Journal on Selected Topics in Signal Processing*, 3(5), 821–831. <https://doi.org/10.1109/JSTSP.2009.2029191>
- Misra, P. & Enge, P. (2010). *Global Positioning System: Signals, Measurements, and Performance* (2nd ed.). Lincoln, MA: Ganga-Jamuna Press.
- Ozsoy, K., Bozkurt, A., & Tekin, I. (2013). Indoor positioning based on global positioning system signals. *Microwave and Optical Technology Letters*, 55(5), 1091–1097. <https://doi.org/10.1002/mop.27520>
- Pages, G. & Vilà-Valls, J. (2019). UWB-based indoor navigation with uncertain anchor nodes positioning. *Proc. of the 32nd International Technical Meeting of the Satellite Division of the Institute of Navigation (ION GNSS+ 2019)*, Miami, FL, 2598–2610. <https://doi.org/10.33012/2019.17060>
- RTCA SC-159. (2006). *Minimum Operational Performance Standards (MOPS) for GPS Local Area Augmentation System Airborne Equipment*. RTCA Document Number DO-229D.
- Saab, S. S., & Nakad, Z. S. (2011). A standalone RFID indoor positioning system using passive tags. *IEEE Trans. on Industrial Electronics*, 58(5), 1961–1970. <https://doi.org/10.1109/TIE.2010.2055774>
- Shin, B., Lee, J. H., Lee, T., & Kee, C. (2019). LTE signal based vehicle localization in indoor parking lot using mobile phone. *Proc. of the 32nd International Technical Meeting of the Satellite Division of the Institute of Navigation (ION GNSS+ 2019)*, Miami, FL, 378–415. <https://doi.org/10.33012/2019.17036>
- Syed, U. B., & Arslan, T. (2011). 3-Dimensional approach to WiFi indoor positioning. *Proc. of the 24th International Technical Meeting of the Satellite Division of the Institute of Navigation (ION GNSS 2011)*, Portland, OR, 2861–2865.
- Tang, H. & Kim, D. (2010). Active RFID indoor positioning and navigation based on probability method. *Proc. of the 23rd International Technical Meeting of the Satellite Division of the Institute of Navigation (ION GNSS 2010)*, Portland, OR, 3388–3397.

- Vervisch-Picois, A. & Samama, N. (2009). Interference mitigation in a repeater and pseudolite indoor positioning system. *IEEE Journal on Selected Topics in Signal Processing*, 3(5), 810–820. <https://doi.org/10.1109/JSTSP.2009.2027805>
- Yan, J., Tiberius, C. C. J. M., Bellusci, G., & Janssen, G. J. M. (2013). Non-line-of-sight identification for indoor positioning using ultra-wideband radio signals. *NAVIGATION*, 60(2), 97–111. <https://doi.org/10.1002/navi.31>
- Zhang, J., Li, B., Dempster, A. G., & Rizos, C. (2010). Evaluation of high sensitivity GPS receivers. *2010 International Symposium on GPS/GNSS*, 410–415.

How to cite this article: Park M, Han J-H, Kim O-J, Kim J, Kee C. One-way deep indoor positioning system for conventional GNSS receiver using paired transmitters. *NAVIGATION*. 2021;68:601–619. <https://doi.org/10.1002/navi.436>

APPENDIX: CONDITIONS OF TRANSMITTERS' INTERVAL

In Subsection 3.1, we mentioned that the early and late values are always present in sections (2) and (4), respectively, when the distance between two transmitters is within 0.25 chip. This appendix explains the reason. First, the offset of two autocorrelations means the difference of the pseudoranges as follows:

$$\Delta\tau^i = \tau_{s1}^i - \tau_{s2}^i = \frac{1}{\lambda_{CA}} (\rho_{s1}^i - \rho_{s2}^i). \quad (\text{A1})$$

Here, λ_{CA} is the wavelength of the coarse/acquisition code, approximately 300 m. Second, the difference of the pseudoranges can be up to twice the distance between the two transmitters. Figure A1 shows the environment when there is a maximum difference in the pseudoranges. The environment is when a satellite is located in line with the two transmitters, and the user is at the position of trans-

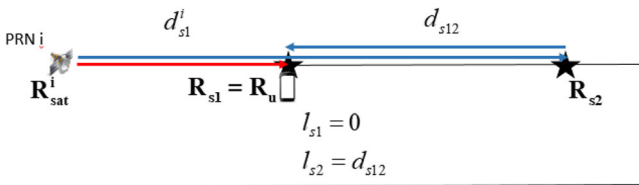


FIGURE A1 Environment when the difference of pseudoranges has the maximum value [Color figure can be viewed in the online issue, which is available at wileyonlinelibrary.com and www.ion.org]

mitter 1.

$$\begin{aligned} \rho_{s1}^i &= (\mathbf{R}_{\text{sat}}^i - \mathbf{R}_{s1}) \cdot \mathbf{e}^i + l_{s1} = d_{s1}^i \\ \rho_{s2}^i &= (\mathbf{R}_{\text{sat}}^i - \mathbf{R}_{s2}) \cdot \mathbf{e}^i + l_{s2} \\ &= (d_{s1}^i + d_{s12}) + d_{s12} = d_{s1}^i + 2d_{s12} \\ \rho_{s1}^i - \rho_{s2}^i &= (\mathbf{R}_{s2} - \mathbf{R}_{s1}) \cdot \mathbf{e}^i + (l_{s1} - l_{s2}) \\ \max(|\Delta\tau^i|) &= \max\left(\left|\frac{1}{\lambda_{CA}} (\rho_{s1}^i - \rho_{s2}^i)\right|\right) = 2d_{s12} \end{aligned} \quad (\text{A2})$$

In Subsection 3.1, the theoretical prompt value is derived, as expressed in Equation (5), when the early and late values are present in sections (2) and (4), respectively. To satisfy the necessary and sufficient conditions, we derive the range of $\Delta\tau^i$ in which early and late values are always present in sections (2) and (4), respectively, when the theoretical prompt is derived as shown in Equation (5). The condition of $\Delta\tau^i$ is derived by changing α from zero to infinity. The conditions for the early to exist in Section (2) are as follows:

$$\begin{aligned} \hat{\tau}_E^i = \hat{\tau}^i - 0.5 &= \frac{\alpha}{1 + \alpha} \Delta\tau^i - 0.5 \\ -1 &\leq \frac{\alpha}{\alpha + 1} \Delta\tau^i - 0.5 \leq \Delta\tau^i \end{aligned} \quad (\text{A3})$$

The inequality on the left is as follows:

$$\begin{aligned} -1 &\leq \frac{\alpha}{\alpha + 1} \Delta\tau^i - 0.5 \\ i) \alpha &\approx 0 \\ -1 &\leq 0 \cdot \Delta\tau^i - 0.5 \quad (\text{trivial case}) \\ ii) \alpha &\approx \infty \\ -1 &\leq \Delta\tau^i - 0.5 \\ -0.5 &\leq \Delta\tau^i \end{aligned} \quad (\text{A4})$$

The inequality on the right is as follows:

$$\begin{aligned} \frac{\alpha}{\alpha + 1} \Delta\tau^i - 0.5 &\leq \Delta\tau^i \\ i) \alpha &\approx 0 \\ 0 \cdot \Delta\tau^i - 0.5 &\leq \Delta\tau^i \\ -0.5 &\leq \Delta\tau^i \\ ii) \alpha &\approx \infty \\ \Delta\tau^i - 0.5 &\leq \Delta\tau^i \quad (\text{trivial case}) \end{aligned} \quad (\text{A5})$$

As mentioned in Subsection 3.1, $\Delta\tau^i$ is a negative value. Considering all cases, the conditions for the early value to

exist in Section (2) regardless of α are as follows:

$$\begin{aligned} -0.5 &\leq \Delta\tau^i \leq 0 \\ |\Delta\tau^i| &\leq 0.5 \text{ [chip]} \end{aligned} \quad (\text{A6})$$

Because the interval between early and late values is one chip, the late value is naturally present in Section (4).

Therefore, summing Equations (A2) and (A6), the distance between two transmitters should be up to 0.25 chip, that is, approximately 75 m.

$$\begin{aligned} \max(|\Delta\tau^i|) &= 2d_{s12} \leq 0.5 \text{ [chip]} \\ \therefore d_{s12} &\leq 0.25 \text{ [chip]} \approx 75 \text{ [m]} \end{aligned} \quad (\text{A7})$$